

## AERODYNAMIC SHAPES DESIGN ON THE BASE OF DIRECT NEWTON TYPE OPTIMIZATION METHOD

**A.V. Grachev\***, **A.N. Kraiko\*\***, **S.A. Takovitskii\***

**\*Central Aerohydrodynamic Institute (TsAGI),**

**\*\*Central Institute of Aviation Motors (CIAM), Russian Federation**

**Keywords:** *aerodynamic shapes, optimization, local linearization, aerodynamic drag*

### Abstract

*The efficient direct optimization method is developed for aerodynamic shapes design at subsonic and supersonic flow regimes. The method combines Newton based algorithm with CFD modeling and is capable of handling large number of design variables. Aerodynamic drag is considered as the objective function minimized under volume and overall dimensions constraints. The efficiency of the method is demonstrated on examples of two-dimensional and axisymmetric aerodynamic shapes design.*

### 1 General Introduction

The present state of the art of computing, methods of mathematical modeling and optimization makes it possible to solve different problems concerning the choice of rational aerodynamic shapes [1, 2]. The ill conditionality of the aerodynamic optimization problem is a matter of difficulty. The number of objective function evaluations increases dramatically with increase of design variables number. To improve reliability of the optimization method and to accelerate the convergence it is proposed elimination of numerical determination of the objective function derivatives. A quadratic form describing dependence of drag on the geometrical parameters is obtained on the basis of a local analysis of the load distribution on the optimized aerodynamic shape. It gives approximations to the true Hessian matrix and the gradient vector of the objective function and the constraints. Newton type method determines shape variations that enable the aerodynamic performance to be improved and ensures a near

to quadratic rate of convergence to the optimum. The variations are utilized and checked in exact solution. A fast convergence to the optimum in case of the large number (more than 100) of the variables is provided.

For the first time the efficiency of the local linearization procedure was demonstrated on example of supersonic aircraft wing optimization [3]. Assuming small perturbation of supersonic flow the pressure change at given surface point is connected with shape deformation in its vicinity. The elementary assessment of pressure variation could be obtained from the simple wave theory for small disturbances. The spatial movement of the surface element requires turn of velocity vector on an angle of deformation so that it remains parallel to the element plane. The turn of the flow results in the pressure variation. A summation of the aerodynamic loading over all elements of the surface leads to a quadratic approximation of the objective function.

### 2 Method of Local Linearization

Applicability of the local linearization approach is expanded to subsonic and transonic regimes by means of utilization of Riemann invariants at non-stationary conditions. The variation of the pressure on the surface element is related with its spatial displacement.

The direct method combines the solution of the direct problem, i.e. the calculation of the flow parameters and distribution of aerodynamic loads, and the solution of the optimization problem, i.e. the determination of the shape variation that is aimed at improving aerodynamic performance. To enhance the

efficiency of the method it is proposed to use a simplified formulation of the problem at the stage of the shape variation determination. The local linearization leads to a linear approximation of the relation between the variations of gas-dynamic functions and geometrical parameters. The objective function is approximated by a quadratic form for which the gradient, the matrix of second derivatives, and the extremum location are found. At the final stage the established variations of the shape are checked in the numerical calculation.

Explain the concept of local linearization. Conventional linearization of the government equations is performed for the perturbations of the uniform flow which are generated by the body. In case of local linearization we use data on the flow field near the body, obtained theoretically or by means of the numerical modeling. Further, in the neighborhood of each element of the optimized surface flow parameters are averaged. The plane defined by the velocity vector and the normal to the surface element is allocated. The local linearization is performed in this plane relative to the averaged flow parameters. The result is the linear dependence between the variations of geometrical parameters and gas-dynamic functions.

Consider subsonic and supersonic flow past a diamond-shaped airfoil. In the case of supersonic flow, the linearization is reduced to the Ackeret's formula and pressure on the surface element is determined by the inclination of this element.

According to the linear theory for thin symmetric bodies ( $c/b \ll 1$ ) located at zero angle of attack, the pressure coefficient is determined by the integral

$$c_p(x) = \frac{2}{\pi\sqrt{1-M^2}} \int_0^b \frac{y'(\xi)}{\xi-x} d\xi$$

Here  $y'$  is the first derivative of the ordinate, and the integration is performed along the longitudinal coordinate in an improper sense,  $c$  and  $b$  – the thickness and the chord of the airfoil,  $M$  – the Mach number at free stream.

The pressure distribution on the airfoil is symmetrical relative to the midlength section. In subsonic flow the pressure at each point of the surface depends on the inclination of the surface at all points of the airfoil and local linearization is not applicable.

Let's complicate the problem and consider the process of subsonic flow stabilization over time. The characteristic quantity of time is determined by the ratio of the airfoil chord length to the flow velocity. In a fairly wide range of time, up to its relative value equal to  $Vt/b=0.2$ , the feature of locality is evident (Fig. 1). The pressure change is determined by the change in the slope of the surface element. The analogy with supersonic flows is traced. Further progression on time breaks this effect. Nevertheless, it is possible to conclude that the non-stationary local linearization is applicable.

The non-stationary local linearization method considers the change in the spatial position of the element as its movement into or moving-out a gas, similar to that of flat piston. Piston velocity  $\Delta V$  is determined by the projection of the vector of the average velocity to the surface normal, corresponding to a new position of the element. A pressure change  $\Delta p$  on the element is connected with the geometric parameters through the Riemann invariants

$$\Delta p = \pm \rho a \Delta V$$

Here  $\rho$  is the density and  $a$  is the sound speed.

Thus, it is possible to determine the quadratic approximation of the objective function and the shape variation, which reduces the objective function for a finite interval of time. The procedure that combines the process of flow stabilization on time and the optimization of aerodynamic shape is implemented. As optimization iterations are completed, the shape variations are reduced and the flow parameters are settled.

### 3 Computational Algorithm

Software implementation of the optimization method is extremely automated. The program set contains three main blocks: the optimization

block, the block of processing geometric data and mesh generation, and the block of numerical flow simulation. The research is conducted on a structured mesh, which is analyzed for the utility of modifications to improve the cells orthogonality. An optimization iteration cycle takes up to 10 direct flow calculations. There is a possibility of an additional variation of the aerodynamic shape in the direction defined by the gradient vector of the objective function.

The initial aerodynamic shape is supplied to the module of processing and generation of the computational grid. Then the numerical simulation of the flow is carried out. The flow parameters are used in the local linearization to determine the shape variations intended for improvement of aerodynamic characteristics. The optimization process is a cyclic one.

In the present study the optimization algorithm is realized on the base of the Ansys Fluent. The flow fields and the aerodynamic pressure loading are calculated within the framework of models based on Euler equations and Reynolds averaged Navier-Stokes equations.

#### 4 Axisymmetric Forebody Optimization

Two local linearization procedures are compared on the example of axisymmetric forebody optimization. The aerodynamic drag (wave drag due to volume) is minimized at zero angle of attack. The results for forebodies with lengthening  $\lambda=2\div 4$  at Mach numbers  $M=2\div 6$  are obtained. The optimization problem is formulated as finding the minimum of the function of many variables

$$c_D = \min$$

The forebody generatrix is partitioned into a set of segments. Moving these segments one can model the diversity of forebody geometry. The nodal points are condensed to the forebody apex. Geometrical parameters are stated as displacements of the nodal points in the normal direction to the axis of symmetry. The number of the geometry parameters is 99. The truncated cone is taken as the initial forebody.

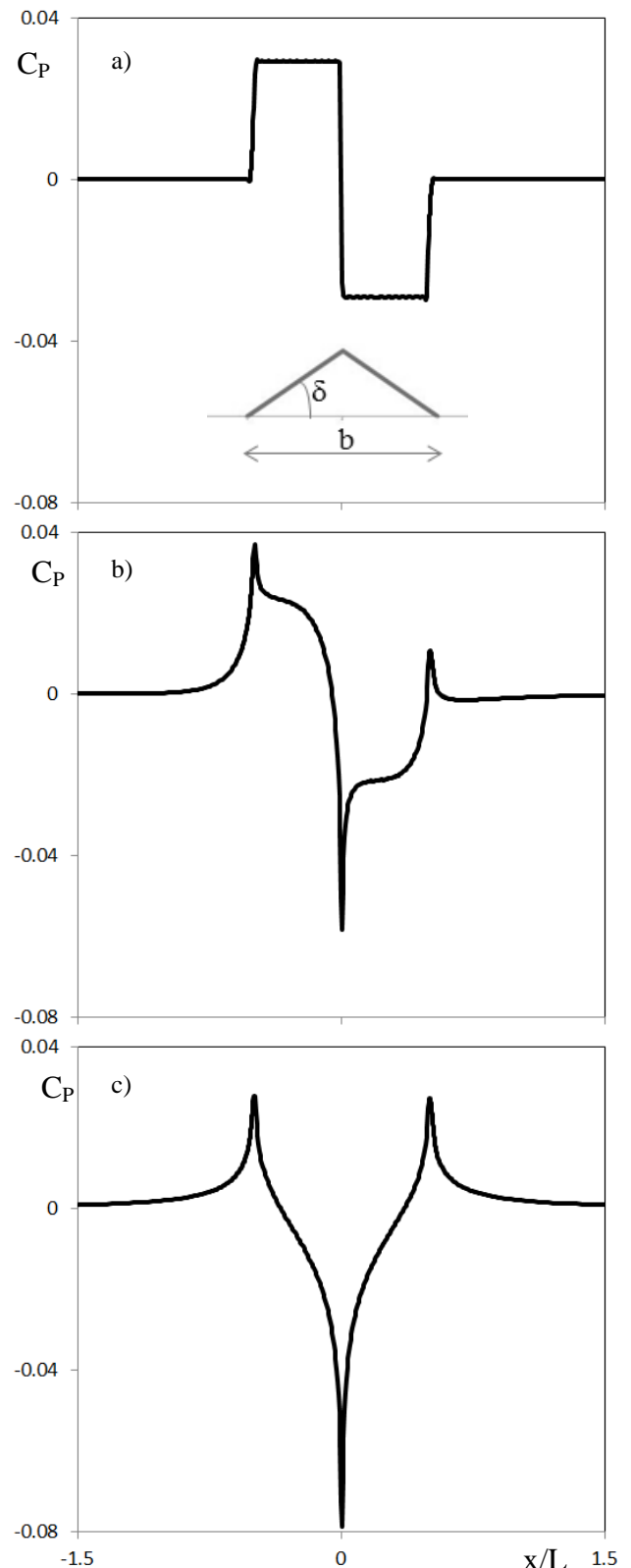


Fig. 1 Pressure coefficient distribution ( $M=0.6$ ,  $\delta=0.5^\circ$ ): a)  $Vt/b=0.002$ , b)  $Vt/b=0.2$ , c)  $Vt/b=20$

At each iteration of shape variation, the flow parameters calculation is performed up to stationary solution. The calculations are performed on block-structured computational grid. To ensure a high degree of orthogonality of the nodes near the surface the procedure of smoothing the grid is implemented. The grid is condensed to the surface of the body.

The investigation shows a fast convergence of the optimization process. Number of the direct calculations is not greater than 30. The variation of the wave drag coefficient  $C_D$  on the number  $It$  of performed optimization iterations is presented in Fig.2 for following conditions: Mach number  $M=2$ , lengthening  $\lambda=2$ .

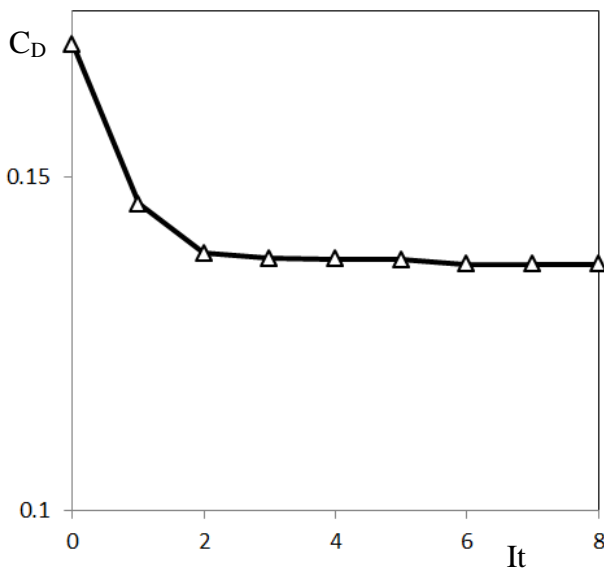


Fig. 2 Drag coefficient variation during optimization process ( $M=2, \lambda=2$ )

Fig. 3 presents the comparison of the forebodies: the original forebody (truncated cone), the forebody found after the first optimization iteration and the optimal forebody. It is seen that after one or two iterations the search path enters the neighborhood of the optimum.

It is established that the optimal forebodies have flat forward faces and near to power-law generatrix. The optimal shapes of forebodies of small lengthening differ significantly from the shapes defined on the base of the Newton pressure equation. On values of drag relative

difference exceeds 25%. The radius of the front face of the Newton forebody is twice smaller.

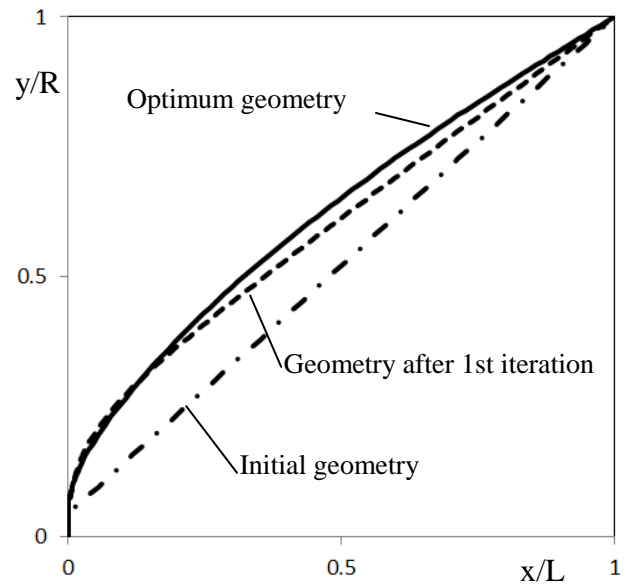


Fig. 3 Nose contours comparison ( $M=2, \lambda=2$ )

The results of the presented study are in good agreement with results obtained by other optimization methods. For example, in [4] the problem is solved by variational method, near-optimal forebodies, which have a power low generatrix and a front flat face, are studied in [5].

### 5 Airfoil Optimization

From the field of subsonic aerodynamics the problem of increasing the critical Mach number is considered. A symmetrical airfoil, which has a fixed nose and tail parts, is investigated. Flow over the airfoil is in keeping with the Ryabushinsky scheme. The conditions of the problem are taken from [6]: the nose and tail wedges length is 20% of the airfoil chord length  $b$ , wedge semiangle is  $22.15^\circ$ . It is required to construct the central part of the airfoil, that ensures the achievement of sonic flow conditions at the free stream Mach number  $M=0.672$ . A mean-square residual on the Mach number on the optimized surface is taken as the objective function  $F$

$$F = \left[ \frac{\sum (M-1)^2 l_i}{\sum l_i} \right]^{0.5} = \min$$

Here  $l$  is length of the airfoil segment.

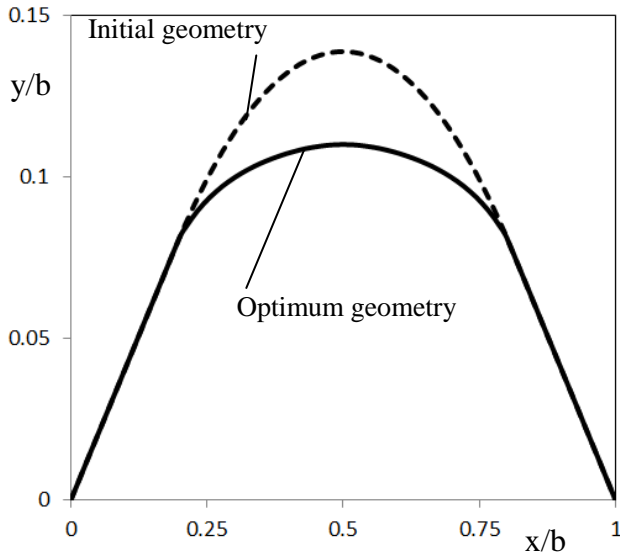


Fig. 4 Airfoils comparison

The contour of the airfoil is represented by a set of segments. Varied parameters are the coordinates of the node points of the segments. At each optimization iteration, the relative value of the time step is  $Vt/b=2$ .

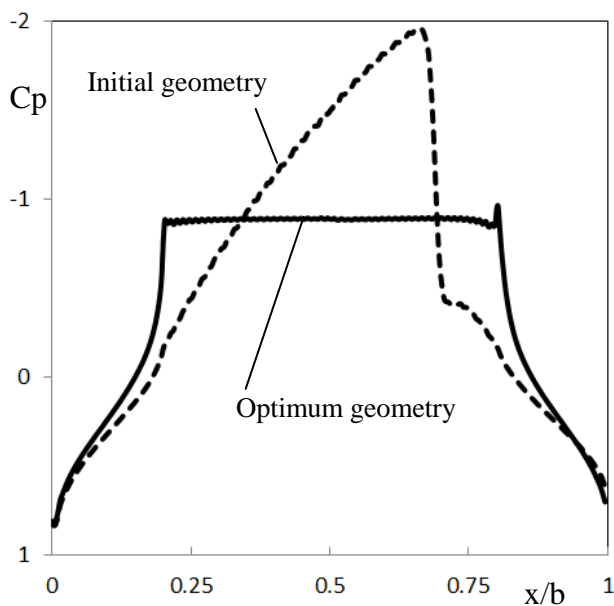


Fig. 5 Pressure coefficient distribution on airfoil surface

The calculations are performed on structured computational grid. The shape variation of the airfoil during the optimization process is shown in Fig. 4. The initial and optimum airfoils are compared on pressure coefficient and Mach number distributions on the airfoil surface and in the flow field. Flow over the initial airfoil is characterized by the presence of a supersonic flow region. The supersonic region is bounded by a strong shock wave. The optimal airfoil provides a flat distribution of gas-dynamic parameters in the central part (Fig. 5).

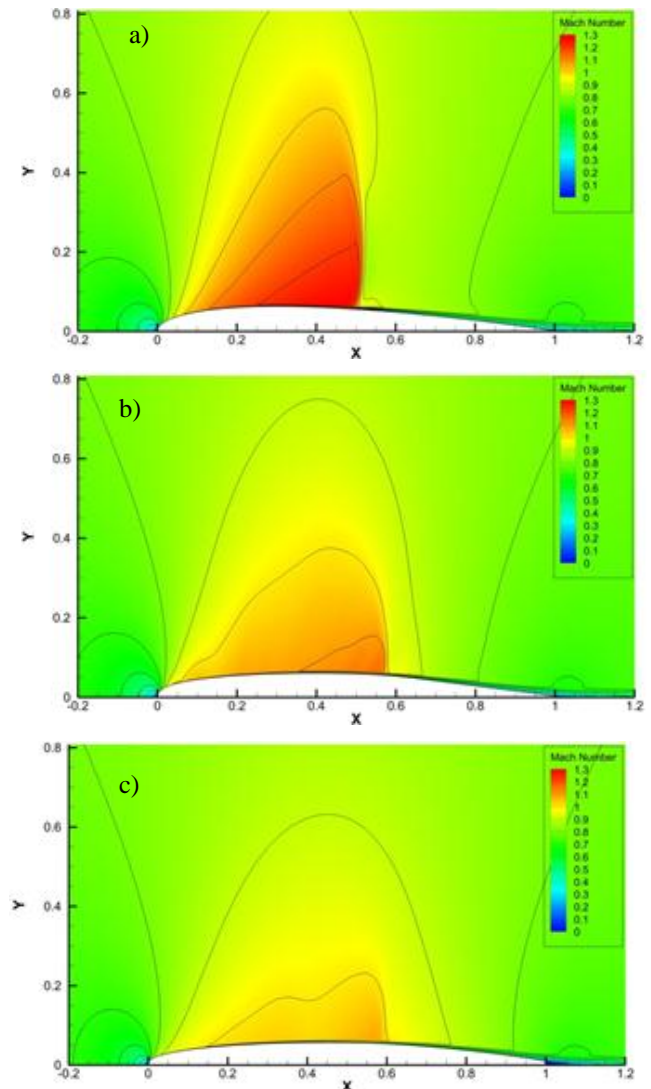


Fig. 6 Mach number contours ( $M=0.8, Re_b=9 \cdot 10^6$ )  
a) NACA-0012  
b) NASA SC(2)-0012  
c) optimum airfoil



The optimization of airfoils with low aerodynamic drag is performed in transonic speeds range. The aerodynamic drag coefficient  $c_D$  is minimized at zero angle of attack. An additional geometrical constraint is imposed on the area of the airfoil  $S$

$$c_D = \min$$

$$S = const$$

NACA-0012 airfoil is taken as the base configuration for symmetrical airfoil profiling. The area of the airfoil is equal to the area of 12% thick symmetrical supercritical airfoil SC(2)-0012 [7]. The minimum of aerodynamic drag and the optimal airfoil shape are found at Mach number  $M=0.8$ . At each optimization iteration, the relative value of the time step is  $Vt/b=2.5$ .

The flow field analysis shows that the velocity distribution on NACA-0012 airfoil is characterized by a shock wave location near the midchord (Fig. 6). The reducing curvature of the optimal airfoil results in the elimination of the flow acceleration ahead the shock wave. The area of the optimal airfoil is redistributed toward the trailing edge in comparison with the airfoil SC(2)-0012 (Fig. 7).

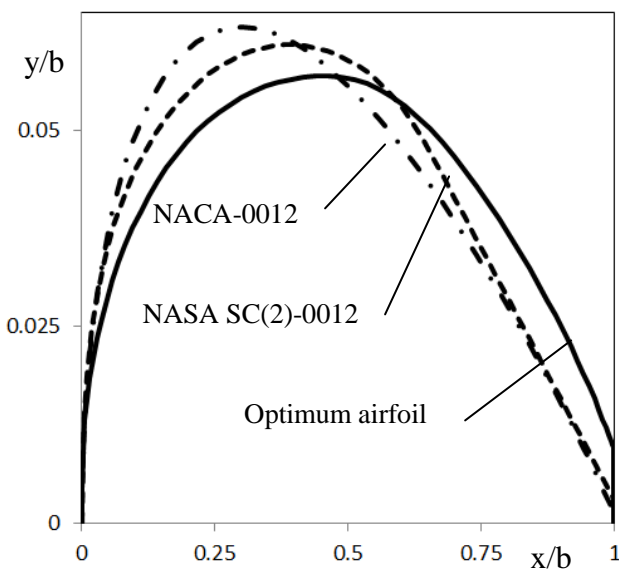


Fig. 7 Airfoils comparison

Comparison of results obtained within the framework of viscous and inviscid models of the flow reveals good agreement in nose part of the airfoil up to the location of the shock wave behind the supersonic flow region. Flow field modeling within the framework of the Euler equations predicts the shock wave located closer to the trailing edge. The results of numerical simulation are in satisfactory agreement with experimental data [7] (Fig. 8).

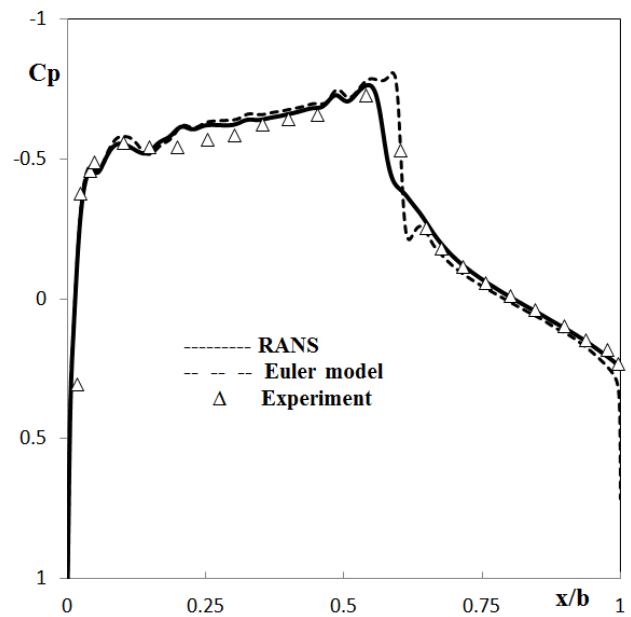


Fig. 8 Pressure coefficient distribution on NASA SC(2)-0012 ( $M=0.8$ ,  $Re_b=9 \cdot 10^6$ )

Comparison of the airfoils on the aerodynamic drag coefficients is shown in fig. 9. The computation research is accomplished for Reynolds number  $Re_b=9 \cdot 10^6$  based on the chord length. Airfoil optimization results in diminution of the aerodynamic drag on more than 50% at Mach number  $M=0.8$ . The relative contribution of the surface friction drag to the airfoil drag is about 60% and decreases with Mach number increasing. As compared to the airfoil SC(2)-0012 the optimal airfoil provides the increase of the critical Mach number on about 0.02. The observed effect is due to the redistribution of the airfoil area towards the trailing edge and to increasing the height of the rear face.

## 6 Conclusion

It was developed the method of aerodynamic shapes optimization on the base of non-stationary local linearization of the relation between gas-dynamic functions and geometrical parameters. The method was tested on examples of construction of axisymmetric forebodies with minimum wave drag and symmetrical airfoils with increased critical Mach number.

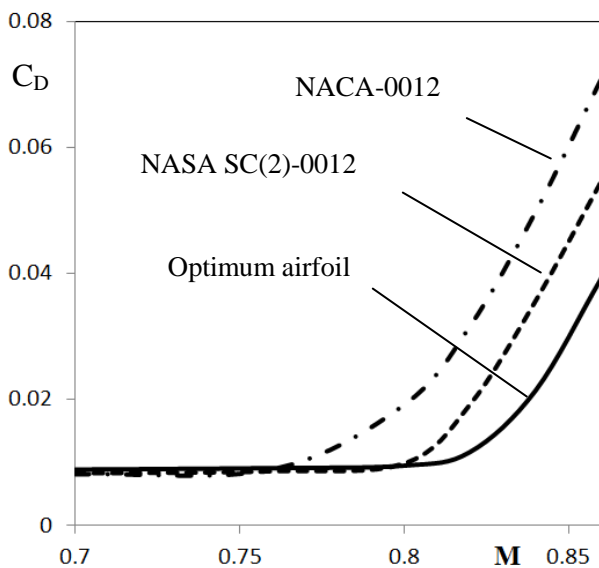


Fig. 9 Drag coefficient on Mach number ( $Re_b=9 \cdot 10^6$ )

## Acknowledgments

This work was partially performed within the ‘High Speed Experimental Fly Vehicles - International’ (HEXAFLY-INT) project fostering International Cooperation on Civil High-Speed Air Transport Research. HEXAFLY-INT, coordinated by ESA-ESTEC, is supported by the EU within the 7th Framework Program Theme 7 Transport, Contract no.: ACP3-GA-2014-620327. The project is also supported by the Ministry of Industry and Trade, Russian Federation. Further information on HEXAFLY-INT can be found on [http://www.esa.int/techresources/hexafly\\_int](http://www.esa.int/techresources/hexafly_int). This research was also supported by the Russian Foundation for Basic Researches, project No. 16-01-00703a.

## References

- [1] Takovitskii S.A. High-speed flying vehicle with hypergeometrically shaped windward aerodynamic surface. *20th AIAA International Space Planes and Hypersonic Systems and Technologies Conference*, 6-9 July 2015, Glasgow, Scotland. AIAA paper 2015-3571, pp. 1-14, 2015.
- [2] Ageev N.D., Pavlenko A.A. Minimization of body of revolution aerodynamic drag at supersonic speeds. *Aircraft Engineering and Aerospace Technology*, Vol. 88, Is. 2, pp. 246 – 256, 2016.
- [3] Takovitsky S.A. Numerical optimization of the wing of a supersonic airplane. *Proc. 23rd Congress of International Council of the Aeronautical Sciences*, 8-13 September, 2002, Toronto, Canada. Paper ICAS 2002-2.3.2, pp. 1-8, 2002.
- [4] Kraiko A.N., Pudovikov D.E., P'yankov K.S., Tillyaeva N.I. Axisymmetric noses of specified elongation which are optimal or close to optimal with respect to wave drag. *Prikl. Mat. Mekh.*, Vol. 67, No. 5, pp. 795-828, 2003.
- [5] Ivanyushkin D.S., Takovitskii S.A. Noses of minimal wave drag in supersonic flow. *Proc. 29th Congress of International Council of the Aeronautical Sciences*, 7-12 September, 2014, St. Petersburg, Russia. Paper ICAS 2014-0181, pp. 1-6, 2014.
- [6] Brutyan M.A., Lyapunov S.V. Optimization of symmetrical flat bodies with the aim of critical Mach number increasing. *Ucheniye zapiski TsAGI*, Vol. XII, No. 5, pp. 10-22, 1981 (in Russian).
- [7] Mineck R.E., Lawing P.L. High Reynolds number tests of the NASA SC(2)-0012 airfoil in the Langley 0.3-meter transonic cryogenic tunnel. *NASA TM-89102*. 1987.

## Contact Author Email Address

c.a.t@tsagi.ru (Takovitskii S.A.)

## Copyright Statement

The authors confirm that they, and/or their company or organization, hold copyright on all of the original material included in this paper. The authors also confirm that they have obtained permission, from the copyright holder of any third party material included in this paper, to publish it as part of their paper. The authors confirm that they give permission, or have obtained permission from the copyright holder of this paper, for the publication and distribution of this paper as part of the ICAS 2016 proceedings or as individual off-prints from the proceedings.